Structural Engineering and Mechanics, *Vol. 56, No. 3 (2015) 473-490*
DOI: http://dx.doi.org/10.12989/sem.2015.56.3.473

Intermediate crack-induced debonding analysis for RC beams strengthened with FRP plates

Peelak Wantanasiri[a] and Akhrawat Lenwari[*]

Department of Civil Engineering, Faculty of Engineering, Chulalongkorn University, Phayathai Road, Pathumwan, Bangkok, Thailand 10330

(Received January 31, 2015, Revised October 26, 2015, Accepted October 28, 2015)

Abstract. This paper presents the analysis of intermediate crack-induced (IC) debonding failure loads for reinforced concrete (RC) beams strengthened with adhesively-bonded fiber-reinforced polymer (FRP) plates or sheets. The analysis consists of the energy release and simple ACI methods. In the energy release method, a fracture criterion is employed to predict the debonding loads. The interfacial fracture energy that indicates the resistance to debonding is related to the bond-slip relationships obtained from the shear test of FRP-to-concrete bonded joints. The section analysis that considers the effect of concrete's tension stiffening is employed to develop the moment-curvature relationships of the FRP-strengthened sections. In the ACI method, the onset of debonding is assumed when the FRP strain reaches the debonding strain limit. The tension stiffening effect is neglected in developing a moment-curvature relationship. For a comparison purpose, both methods are used to numerically investigate the effects of relevant parameters on the IC debonding failure loads. The results show that the debonding failure load generally increases as the concrete compressive strength, FRP reinforcement ratio, FRP elastic modulus and steel reinforcement ratio increase.

Keywords: fiber-reinforced polymers; strengthening; reinforced concrete beams; intermediate crack-induced debonding; bond-slip relationships; fracture mechanics

1. Introduction

Debonding of adhesively-bonded fiber-reinforced polymer (FRP) sheets or plates from the strengthened reinforced concrete (RC) beams is unfavorable and must be considered in the strengthening design. The debonding failures can be classified into two following types: (1) plate-end (PE) debonding and (2) intermediate cracked-induced (IC) debonding. The PE debonding initiates at the plate's cut-off points due to high interfacial shear and normal (peeling) stresses at the plate ends. Design of anchorages to prevent this type of debonding is recommended by the design guides, e.g., ACI 440.2R (ACI 2008). In contrast, the IC debonding initiates at the flexural or flexural-shear cracks between the plate's cut-off points and propagates towards the plate ends. Unfortunately, the IC debonding failure cannot be prevented by any anchorage means. To mitigate the debonding failure, ACI 440.2R (ACI 2008) currently suggests the use of FRP strain limit, a

∗Corresponding author, Associate Professor, E-mail: akhrawat.l@chula.ac.th
[a]Graduate Student

http://www.techno-press.org/?journal=sem&subpage=8 ISSN: 1225-4568 (Print), 1598-6217 (Online)

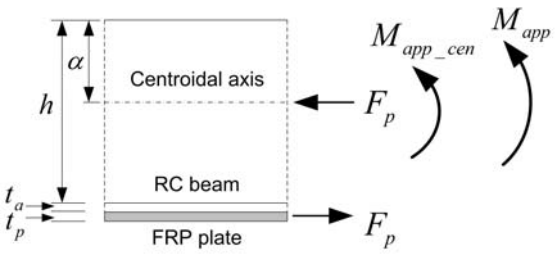

Fig. 1 Internal forces in FRP-strengthened beam section (adapted from Achintha and Burgoyne 2008)

strain value which is less than the design rupture strain of FRP.

The analyses of plate debonding have been performed by many past research works (e.g. Täljsten 1997, Malek *et al*. 1998, Leung 2001, Smith and Teng 2001, Teng *et al*. 2003, Liu *et al*. 2007, Lu *et al*. 2007, Wu and Niu 2007, Achintha and Burgoyne 2008, Dai *et al*. 2008, Gunes *et al*. 2009, Ombres 2010, Zhang and Teng 2010, Hao *et al*. 2012, Choi *et al*. 2013, Wang *et al*. 2013, Guan *et al*. 2014). The existing models for predicting the debonding strength use the strength-based or fracture-mechanics-based approaches (Teng *et al*. 2002, Said and Wu 2008, Achintha 2009).

This paper presents the analysis of IC debonding failure in RC beams strengthened with FRP plates or sheets. First, the section analysis that considers the effect of concrete's tension stiffening on the moment-curvature relationships of the FRP-strengthened sections is described. Then, the applications of energy release method to the debonding analysis of FRP-to-concrete bonded joints and FRP-strengthened RC beams are presented. For a comparison purpose, the failure loads are also predicted using a simple ACI method. In the ACI method, the onset of debonding is assumed when the value of FRP strain is equal to the debonding strain limit. The tension stiffening effect is neglected in developing a moment-curvature relationship. A total of 28 specimens from previous 11 experimental works are chosen in this study. Finally, both energy release and ACI methods are used to investigate the effects of relevant parameters including the concrete compressive strength, FRP reinforcement ratio, FRP elastic modulus and steel reinforcement ratio on the predicted debonding failure loads.

2. Flexural analysis for FRP-strengthened RC beams

The flexural analysis for FRP-strengthened RC beams includes the section analysis for the moment-curvature relationship and virtual work analysis for the load-displacement relationship.

Achintha and Burgoyne (2008) proposed the moment-curvature analysis that includes the tension stiffening effects for the FRP-strengthened RC beam section. Fig. 1 shows the internal forces in the FRP-strengthened beam section. Conceptually, the axial FRP force (F_p) is considered to be a compressive prestressing force applied to the RC beam section. Three different axes for moment consisting of the centroidal axis (for energy analysis), neutral axis (for strain compatibility condition), and mid-depth axis (for cracking state) are defined. For example, the moment acting on the RC section alone about the centroidal axis (M_{app_cen}) is related to the applied external moment on the strengthened section (M_{app}) by

$$M_{app\_cen} = M_{app} - F_p \times (h + t_a + t_p / 2 - \alpha) \quad (1)$$

where h, t_a , t_p and α are the overall depth of RC section, adhesive layer thickness, FRP thickness, and depth of centroidal axis, respectively.

The compressive stress-strain relationship of concrete is (Park and Paulay 1975)

$$\sigma_c = f_c^{'}\left[\frac{2\varepsilon_c}{\varepsilon_{\max}} - \left\{\frac{\varepsilon_c}{\varepsilon_{\max}}\right\}^2\right] \quad \text{and} \quad \varepsilon_c \le \varepsilon_{\max} \tag{2}$$

$$\sigma_c = f_c^{'}\left[1 - \frac{0.15}{0.004 - \varepsilon_{\max}}\left(\varepsilon_c - \varepsilon_{\max}\right)\right] \quad \text{for} \quad \varepsilon_{\max} < \varepsilon_c \le 0.004 \quad \text{and} \quad \varepsilon_{\max} = \frac{2f_c^{'}}{E_c} \tag{3}$$

where $f_c^{'}$ and E_c are the peak compressive stress and elastic modulus of concrete, respectively.

The tensile stress-strain relationships of uncracked concrete, steel reinforcements and FRP plates are assumed to be linear elastic, elastic-perfectly plastic and linear elastic, respectively.

The moment-curvature relationship of a typical under-reinforced RC beam section strengthened with the FRP plate can be divided into three cracking stages as follows: (a) uncracked section (b) partially-cracked section and (c) fully-cracked section. The cracking moment (M_{cr}) is the moment that causes the tensile strain in the extreme concrete layer to equal to $\varepsilon_r = f_r/E_c$, where f_r and E_c are the modulus of rupture and elastic modulus of concrete, respectively. The yield moment (M_y) is the moment that causes the tensile steel reinforcements to start to yield, i.e., steel strain equals to the yield strain. And, the ultimate moment (M_{ult}) is the moment that causes the compressive strain in concrete to reach the ultimate strain after steel reinforcements yield.

In the first stage, the applied moment about the mid-depth axis is less than M_{cr}. An uncracked section is assumed. The moment-curvature relationship is assumed to be linear. In the second stage, the applied moment about the mid-depth axis is between M_{cr} and M_y. A partially-cracked section is assumed. In the final stage, the applied moment about the mid-depth axis is between M_y and M_{ult}. A fully-cracked section is assumed.

In the section analysis, the value of FRP force (F_p) is adjusted until the strain compatibility condition is satisfied. Once the moment-curvature relationship is obtained, the load-deflection relationship is constructed using the principle of virtual work (Lenwari *et al*. 2005, Lenwari and Thepchatri 2009). A comparison of the predicted results with available experimental data has shown good agreements (Wantanasiri and Lenwari 2011).

3. Debonding analysis of FRP-to-concrete bonded joints

3.1 Energy release method

Täljsten (1996) applied the linear elastic fracture mechanics to a bonded joint of width "*b*" having a crack of length "*a*" shown in Fig. 2. The basic assumptions are as follows: (1) both adherends and adhesive are homogenous, isotropic and linear elastic materials (2) adhesive resists only shear forces (3) adherends and adhesive have constant thickness and width along the bondline.

From the energy balance, the following fracture criterion for debonding can be derived

$$\frac{d}{dA}\left(F - U_e\right) \ge \frac{dW}{dA} \tag{4}$$

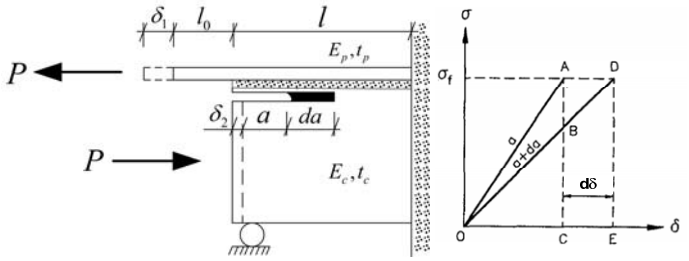

Fig. 2 Single-lap bonded joints with crack of length "*a*" (adapted from Täljsten 1996)

Where F=work done by the external force, U_e=stored elastic energy, W=energy for crack propagation, and A=crack area (=ba). The term on the left and right hand sides represent the "energy release rate (G)" and "crack resistance force or fracture energy (G_f)", respectively.

The work done by the external force is

$$F = P\delta \tag{5}$$

and the stored elastic energy is

$$U_e = \frac{1}{2}P\delta = \frac{1}{2}P^2C \tag{6}$$

where C is the joint compliance, or the inverse of the joint stiffness, (δ=PC). The relative displacement at the load application points is $\delta=\delta_1+\delta_2$.

Fig. 2 also depicts the stress-displacement curve of a bonded joint during action of force "P". As the crack extends by an amount da, the relative displacement at the load application points is increased by an amount $d\delta$. By substituting Eqs. (5) and (6) into Eq. (4), the energy release rate is

$$G = \frac{P^2}{2b}\frac{\partial C}{\partial a} \quad \text{or} \quad P = \sqrt{2bG\Big/\frac{\partial C}{\partial a}} \tag{7}$$

where P and δ are the external force and displacement, respectively. The compliance is given by

$$C = \frac{l_0 + a}{E_p A_p} + \frac{a}{E_c A_c} \tag{8}$$

$$\frac{\partial C}{\partial a} = \frac{1}{E_p A_p} + \frac{1}{E_c A_c} \tag{9}$$

where l_0, E_pA_p and E_cA_c are the extended length of the FRP plate, axial rigidity of FRP plate, and axial rigidity of concrete prism, respectively.

By substituting Eq. (9) into Eq. (7) and assuming that the axial rigidity of concrete is much higher than that of the FRP plate, i.e., neglecting the term $1/E_cA_c$, the maximum transferable load (P_{max}) limited by interfacial fracture is

$$P_{\max} = b\sqrt{2G_f E_p t_p} \tag{10}$$

where G_f and t_p are the fracture energy and thickness of FRP plate, respectively.

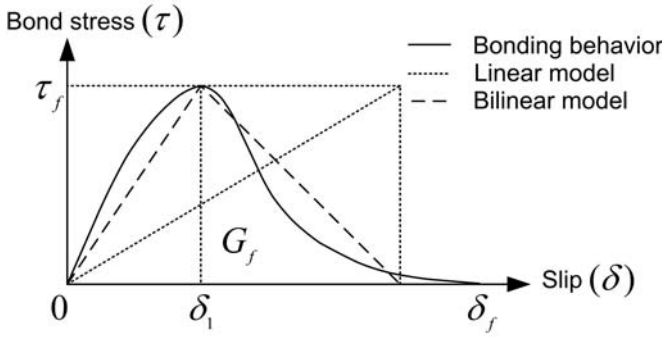

Fig. 3 Nonlinear v.s. linear bond stress-slip relationships

3.2 Bond-slip relationships

The bond stress-slip relationship influences the response of the bonded joint including the shear stress distribution along the interface and the load-displacement response of the bonded joints (Wu *et al*. 2002, Yuan *et al*. 2004, Dai *et al*. 2005).

Fig. 3 shows a nonlinear bond stress-slip relationship for FRP-to-concrete bonded joints. Simplification may be made using linear models with or without softening behavior as represented by the dashed and dotted lines, respectively. The bond shear strength is denoted by τ_f. The fracture energy (G_f) that is required to cause an interfacial fracture corresponds to the area under the bond-slip curve.

Nakaba *et al.* (2001) conducted a series of bond tests on concrete prisms reinforced with bonded FRP laminates. The experimental results showed that the bond shear strength increases with concrete compressive strength (f_c'). The proposed nonlinear bond stress-slip model is

$$\tau = \tau_f \left[\frac{\delta}{\delta_1} \cdot \frac{n}{(n-1)+\left(\frac{\delta}{\delta_1}\right)^n} \right] \tag{11}$$

$$\tau_f = 3.50 f_c'^{0.19} \quad \text{(MPa)} \tag{12}$$

where τ, τ_f, δ, δ_1 and n are bond shear stress (MPa), bond shear strength (MPa), slip (mm), slip at τ_f (=0.065 mm) and constant (=3), respectively. The applicable range of concrete compressive strength is between 24 and 58 MPa.

The interfacial fracture energy (G_f) which is the area under the local bond stress-slip relationship is

$$G_f = \int_0^\infty \tau d\delta = \int_0^\infty \tau_f \left[\frac{\delta}{\delta_1} \cdot \frac{n}{(n-1)+\left(\frac{\delta}{\delta_1}\right)^n} \right] d\delta \approx 0.184 \tau_f = 0.644 f_c'^{0.19} \quad \text{(N/mm)} \tag{13}$$

Accordingly, the effective bond length (L_e), which is a distance required for FRP laminates to develop the maximum transferable FRP tensile load (P_{max}) in Eq. (10), is approximated to be (Wu and Niu 2007)

$$L_e \approx \frac{P_{\max}}{\left(\frac{b_p \tau_f}{2}\right)} = \frac{2b_p\sqrt{2G_f E_p t_p}}{b_p \tau_f} = \frac{0.649\sqrt{E_p t_p}}{f_c^{'0.095}} \tag{14}$$

where b_p is the width of FRP plate. A step-by-step procedure of the energy release method is given in Appendix A.

4. Debonding analysis of FRP-strengthened RC beams

4.1 Energy release method

Wu and Niu (2007) proposed a model for predicting the IC debonding failure loads of FRP-strengthened RC beams. It was recognized that the existence of multiple flexural cracks in beams, a condition that is different from a unique localized crack in the case of bonded joints, tends to cause the transfer length to be longer than the case of bonded joints. The distribution of FRP tensile forces along adjacent cracks is also different from the case of bonded joints. The model assumes that the debonding failure occurs when the difference in magnitude between the FRP tensile forces over an equivalent transfer length (L'_e) measured from the maximum moment location (see Fig. 4) reaches the maximum transferable load (P_{max}). By adapting Eq. (10), the debonding load, denoted by P_{deb}, is

$$P_{deb} = P \quad \text{when} \quad f_2 - f_1 \geq b_p\sqrt{2G_f E_p t_p} \tag{15}$$

where f_1 is the FRP tensile force at a section located away from the main localized crack, i.e., midspan, by a shorter distance of equivalent transfer length and yielding zone of steel reinforcements (see Fig. 4), and f_2 is the FRP tensile force at the main localized crack.

The equivalent transfer length, L'_e is defined as an increased effective bond length that considers the effects of distributed cracks and is proposed to be

$$L_e^{'} = \alpha L_e \tag{16}$$

where α is the factor that accounts for effects of multiple cracks on the transfer length (=2).

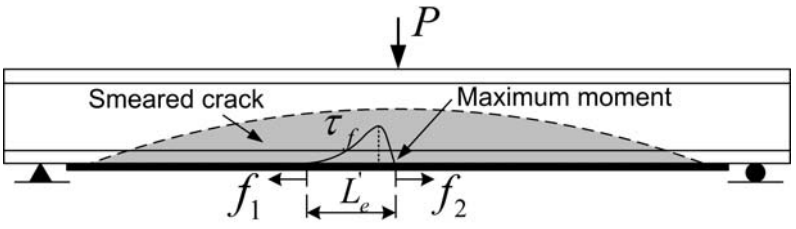

Fig. 4 Definition of parameters in model of Wu and Niu (2007)

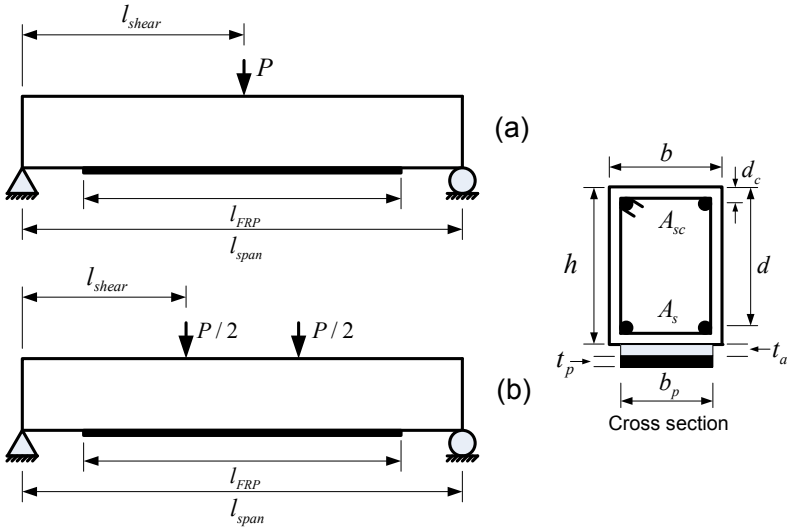

Fig. 5 Schematic representation of FRP-strengthened RC beams subjected to (a) Three-point bending (b) Four-point bending

4.2 ACI Method (ACI 440.2R-08)

ACI 440.2R (ACI 2008) suggests the use of FRP strain limits. The effective strain in the FRP is limited to a value less than the design rupture strain of FRP. In this study, the debonding failure load is predicted when the FRP effective strain (ε_{fe}) reaches the following debonding strain limit (ε_{fd})

$$\varepsilon_{fd} = 0.41\sqrt{\frac{f_c^{'}}{nE_f t_f}} \le 0.9\varepsilon_{fu} \tag{17}$$

where n, t_f and E_f are the number of layers, thickness of FRP layer, and elastic modulus of FRP, respectively.

For the ACI method, a simple moment-curvature model which neglects the tension stiffening effects is used. The FRP plate or sheet is regarded as a layer of reinforcement additional to the steel reinforcements. The nonlinear compressive stress distribution in concrete is approximated by an equivalent rectangular stress block. The concrete crushing strain is assumed to be 0.003. The neutral axis location is obtained from the condition of equilibrium of internal forces, i.e., no axial force. Once the neutral axis is located, the moment and curvature are calculated. A step-by-step procedure of the ACI method is given in Appendix A.

5. Comparison of predicted results with previous experimental data

A total of 28 specimens from previous 11 experimental works is chosen in this study. Fig. 5 shows the symbols of geometric, loading, and material parameters of FRP-strengthened RC beams. Table 1 shows the values of the parameters l_{span}, l_{shear}, l_{FRP}, b, h, d, d_c, A_s, A_{sc}, f_{ys}, E_s, $f_c^{'}$, b_p,

Table 1 Values of parameters of FRP-strengthened RC beams in previous experimental studies

Reference	Speci-men	Beam geometry							Steel reinforcement				Concrete	FRP				
		l_{span} (mm)	l_{shear} (mm)	l_{FRP} (mm)	b (mm)	h (mm)	d (mm)	d_c (mm)	A_s (mm^2)	A_{sc} (mm^2)	f_{y_s} (N/mm^2)	E_s (kN/mm^2)	f_c' (N/mm^2)	b_p (mm)	t_p (mm)	t_a (mm)	f_{pu} (N/mm^2)	Ep (kN/mm^2)
Saadatmanesh and Ehsani (1991)	B	4575	1982.5	4265	205	455	400	55	1013.4	253.4	456	200	35.00	152	6.00	1.5	400	37.2
Kishi *et al.* (1998)	A200-1	2600	1050	2500	150	250	210	40	402.1	402.1	378.2	205.8	24.81	130	0.138	0.636	2480	126.5
	A415-1	2600	1050	2500	150	250	210	40	402.1	402.1	378.2	205.8	24.81	130	0.286	0.636	2480	126.5
	A623-1	2600	1050	2500	150	250	210	40	402.1	402.1	378.2	205.8	24.81	130	0.429	0.636	248	126.5
	C300-1	2600	1050	2500	150	250	210	40	402.1	402.1	378.2	205.8	24.81	130	0.167	0.636	4070	230.5
	C445-1	2600	1050	2500	150	250	210	40	402.1	402.1	378.2	205.8	24.81	130	0.248	0.636	4070	230.5
Spadea *et al.* (1998)	A3.1	4800	1800	4700	140	300	263	37	402.1	402.1	435	200	24.00	80	1.20	2	2300	152
Beber *et al.* (1999)	VR5	2349	783	2199	120	250	214	34	157.1	56.5	565	200	33.58	120	0.44	2*	2300	152
	VR7	2349	783	2199	120	250	214	34	157.1	56.5	565	200	33.58	120	0.77	2*	3400	230
	VR9	2349	783	2199	120	250	214	34	157.1	56.5	565	200	33.58	120	1.10	2*	3400	230
Tumialan *et al.* (1999)	A1	2130	1065	2130	150	300	250	-	792	-	427	207	51.70	150	0.165	0.635	3400	230
	A2	2130	1065	2130	150	300	250	-	792	-	427	207	51.70	150	0.330	0.636	3400	230
	A7	2130	1065	2130	150	300	250	-	792	-	427	207	51.70	75	0.330	0.636	3400	230
	C1	2130	1065	2130	150	300	250	-	792	-	427	207	51.70	150	0.165	0.636	3400	230
Chan *et al.* (2001)	B2	4600	1600	4500	250	470	430	40	628.3	402.1	505	200	42.40	150	1.20	2*	3180	181
	B3	4600	1600	4500	250	470	430	40	942.5	402.1	505	200	42.40	150	1.20	2*	3180	181
	B6	4600	1600	3700	250	470	430	40	628.3	402.1	505	200	42.40	150	1.20	2*	3180	181
	B8	4600	1600	3700	250	470	430	40	1256.6	402.1	505	200	42.40	150	1.20	2*	3180	181
Fanning and Kelly (2001)	F4	2800	1100	2800	155	240	203	37	339	226	532	204	80.00	120	1.20	3	2400	155
Rahimi and Hutchinson (2001)	B3	2100	750	1930	200	150	120	30	157.1	100.5	5745	210	40.00	150	0.40	2	1532	127
	B5	2100	750	1930	200	150	120	30	157.1	100.5	5745	210	1.20	150	0.40	2	1532	127
	B7	2100	750	1930	200	150	120	30	157.1	100.5	5745	210	1.80	150	0.40	2	1074	36
Gao *et al.* (2004)	A0	1500	500	1200	150	200	162	27	157.1	100.5	531	200	35.70	75	0.22	2	4200	235
Maalej and Leong (2005)	A5	1500	500	1450	115	146	120	26	235.6	157.1	547	180	42.80	107.8	0.33	0.636	3550	235
	B3	3000	1000	2900	230	292	240	52	942.5	628.3	544	183	42.80	215.6	0.33	0.636	3550	235
	B5	3000	1000	2900	230	292	240	52	942.5	628.3	544	183	42.80	215.6	0.66	0.636	3550	235
	C3	4800	1600	4640	368	467	384	83	2412.7	1608.5	552	181	42.80	368	0.495	0.636	3550	235
Gunes *et al.* (2009)	S2PF7M	1350	450	1270	150	180	150	30	392	142	440	200	41.40	38.1	1.20	2*	2800	165

* Assumed value.

t_p, t_a, f_{pu} and E_p which denote the span length, shear span, length of FRP plate, width of RC beam, depth of RC beam, effective depth of tension steel reinforcements, effective depth of compression steel reinforcements, area of tension steel reinforcements, area of compression steel reinforcements, yield strength of steel reinforcements, elastic modulus of steel reinforcements,

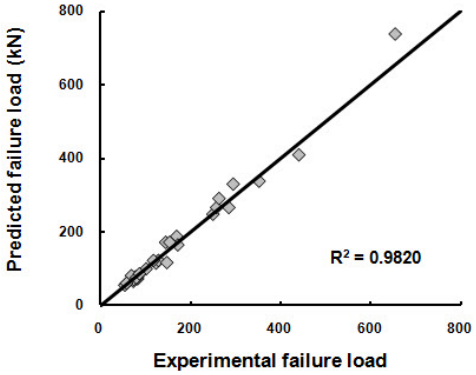

Fig. 6 Experimental v.s. predicted failure loads (an energy release method)

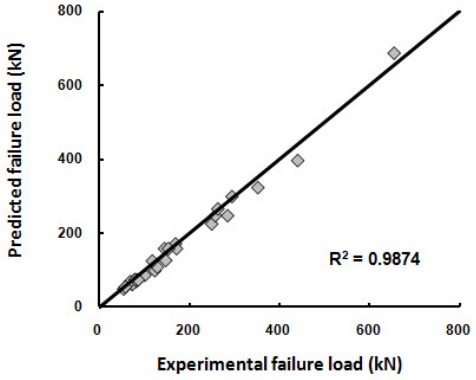

Fig. 7 Experimental failure loads v.s. predicted failure loads (a simple ACI method)

concrete compressive strength, width of FRP, thickness of FRP, thickness of adhesive layer, tensile strength of FRP, and elastic modulus of FRP, respectively.

In all previous experimental studies, the FRP plates were non-prestressed with no anchorage. The failure mode was IC debonding. The FRP materials include GFRP, AFRP, and CFRP with the elastic moduli ranging from 36 to 235 GPa. The span lengths range from 1.35 to 4.8 m. The shear spans range from 0.45 to 1.98 m. The steel reinforcement ratios range from 0.58 to 2.11%. The FRP reinforcement ratios range from 0.06 to 1.13%. The concrete compressive strengths range from 24 to 80 MPa. The RC beam sections range from 115×146 mm (smallest) to 368×467 mm (largest).

Table 2 compares the predicted failure loads by both energy release and simple ACI methods with the experimental results. In the table, P_{exp}, P_{pred} and P_{ACI} denote the experimental failure loads, the predicted failure load by energy release method, and by ACI method, respectively. The comparison results are also plotted in Figs. 6 and 7, respectively. By using the energy release method, the P_{pred}/P_{exp} ratios range from 0.80 to 1.19 with an average value of 1.01 and a standard deviation of 0.09. By using the ACI method, the P_{ACI}/P_{exp} ratios range from 0.80 to 1.09 with an average value of 0.93 and a standard deviation of 0.08. Although the predicted failure loads by the ACI method are conservative in most cases (20 of 28 specimens), a concrete crushing failure mode was predicted in 9 of 28 specimens which did not agree with the test data.

Table 2 Comparison of predicted failure loads with previous experimental results

Reference	Specimen	FRP type	Load configuration	Experimental	Predicted result		P_{ACI}/P_{exp}	P_{pred}/P_{exp}
				P_{exp} (kN)	P_{ACI} (kN)	P_{pred} (kN)		
Saadatmanesh and Ehsani (1991)	B	GFRP	Four point bending	250.0	225.6	249.8	0.90	1.00
Kishi *et al.* (1998)	A200-1	AFRP	Four point bending	74.0	63.4[a]	67.3	0.86	0.91
	A415-1	AFRP	Four point bending	83.4	70.9	74.3	0.85	0.89
	A623-1	AFRP	Four point bending	79.0	74.7	80.0	0.95	1.01
	C300-1	CFRP	Four point bending	79.2	71.4	75.0	0.90	0.95
	C445-1	CFRP	Four point bending	84.0	75.2	80.8	0.90	0.96
Spadea *et al*. (1998)	A3.1	CFRP	Four point bending	74.8	62.7	72.5	0.84	0.97
Beber *et al*. (1999)	VR5	CFRP	Four point bending	102.2	87.2	101.3	0.85	0.99
	VR7	CFRP	Four point bending	124.2	99.8	117.0	0.80	0.94
	VR9	CFRP	Four point bending	12.96	109.5	124.3	0.84	0.96
Tumialan *et al*. (1999)	A1	CFRP	Three point bending	145.6	159.1[a]	173.5	1.09	1.19
	A2	CFRP	Three point bending	169.8	171.9[a]	189.6	1.01	1.12
	A7	CFRP	Three point bending	172.2	159.1[a]	166.4	0.92	0.97
	C1	CFRP	Three point bending	154.4	159.1[a]	173.5	1.03	1.12
Chan *et al*. (2001)	B2	CFRP	Four point bending	285.0	248.1	268.0	0.87	0.94
	B3	CFRP	Four point bending	352.0	323.7	339.6	0.92	0.96
	B6	CFRP	Four point bending	258.0	248.1	268.0	0.96	1.04
	B8	CFRP	Four point bending	440.0	396.7	411.3	0.90	0.93
Fanning and Kelly (2001)	F4	CFRP	Four point bending	118.5	125.8	124.0	1.06	1.05
Rahimi and Hutchinson (2001)	B3	CFRP	Four point bending	55.2	50.4	57.1	0.91	1.03
	B5	CFRP	Four point bending	69.7	70.2	82.9	1.01	1.19
	B7	CFRP	Four point bending	59.1	56.0	62.5	0.95	1.06
Gao *et al*. (2004)	A0	CFRP	Four point bending	80.7	75.9	77.2	0.94	0.96
Maalej and Leong (2005)	A5	CFRP	Four point bending	87.4	75.1[a]	87.9	0.86	1.01
	B3	CFRP	Four point bending	263.5	266.2[a]	292.7	1.01	1.11
	B5	CFRP	Four point bending	294.7	299.5[a]	331.8	1.02	1.13
	C3	CFRP	Four point bending	652.9	686.1[a]	739.6	1.05	1.13
Gunes *et al.* (2009)	S2PF7M	CFRP	Four point bending	148.3	127.2	118.5	0.86	0.80
						Average	0.93	1.01
						Standard deviation	0.08	0.09

[a]concrete crusing failure

6. Effects of parameters on IC debonding failure loads

A parametric study is performed to numerically investigate the effects of relevant parameters on the predicted IC debonding failure loads (P_{pred}) using both energy release and ACI methods. Only the flexural failure modes, i.e., IC debonding, concrete crushing and FRP rupture, are considered.

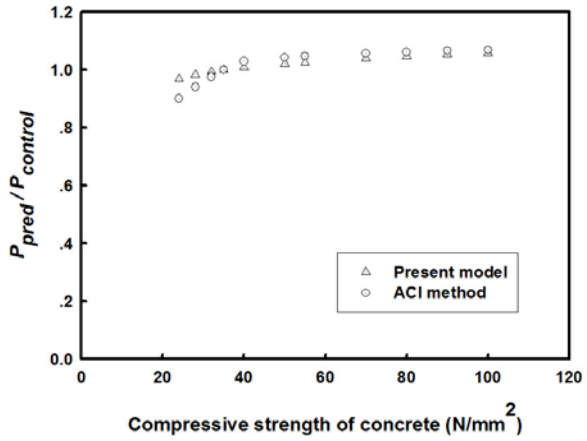

Fig. 8 Effect of concrete compressive strength on $P_{pred}/P_{control}$

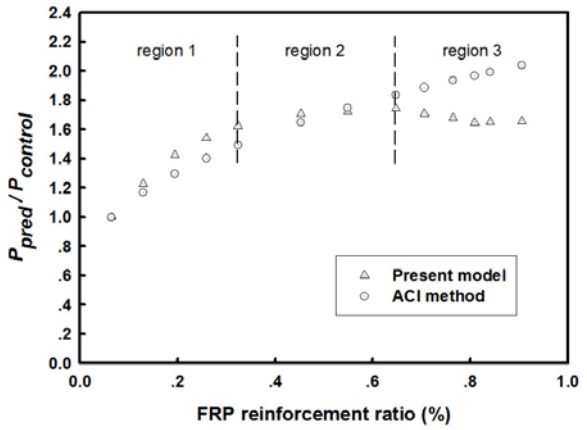

Fig. 9 Effect of FRP reinforcement ratio on $P_{pred}/P_{control}$

The chosen parameters include the concrete compressive strength (f_c'), FRP reinforcement ratio (ρ_f), steel reinforcement ratio (ρ_s), and FRP elastic modulus (E_p). Refer to Fig. 5(b), the control beam has the following parameter values: l_{FRP}=l_{span}=2000 mm, l_{shear}=775 mm, b=150 mm, h=300 mm, d=255 mm, A_{sc}=0 sq.mm., A_s=226 sq.mm. (ρ_s=0.591%), ρ_f=0.065%, $\rho_{balance}$=3.57%, $f_{y\ s}$=400 MPa, E_s=200 GPa, f_c'=35 MPa, b_p=150 mm, t_p=0.165 mm, t_a=0.636 mm, f_{pu}=3550 MPa, and E_p=235 GPa. The predicted debonding failure loads of the control beam ($P_{control}$) are 100.3 and 99.5 kN for the energy release and ACI methods, respectively.

6.1 Concrete compressive strength (f_c')

Fig. 8 shows the effect of concrete compressive strength on the IC debonding failure load as represented by $P_{pred}/P_{control}$ ratio. It was found that the increase in concrete compressive strength increases the debonding load for both energy release and ACI methods. However, the effect is minimal.

6.2 FRP reinforcement ratio (ρ_f)

Fig. 9 shows the effect of FRP reinforcement ratio on the IC debonding failure load as represented by $P_{pred}/P_{control}$ ratio. According to the energy release method, the effect of an amount of FRP reinforcement can be divided into three regions. By increasing an amount of FRP reinforcement, the debonding load significantly increases (the first region), followed by a minimal increase (the second region), and finally a decrease (the third region). For the ACI method, however, the effect of FRP reinforcement is only to increase the debonding load. The predicted behavior is in agreement with the experimental data by Tumialan *et al*. (1999), where the debonding load increases with more FRP reinforcements.

6.3 Steel reinforcement ratio (ρ_s)

Fig. 10 shows the effect of steel reinforcement ratio on the IC debonding failure load as represented by $P_{pred}/P_{control}$ ratio. The debonding load increases with increasing steel reinforcement ratio according to both energy release and ACI methods. The predicted behavior is in agreement with the experimental data by Chan *et al*. (2001). However, if the steel reinforcement ratio is too high, the concrete crushing was found to govern the failure mode of the strengthened beams. The concrete crushing failure load increases with more steel reinforcements.

6.4 FRP elastic modulus

Fig. 11 shows the effect of FRP elastic modulus on the IC debonding failure load as represented by $P_{pred}/P_{control}$ ratio. It was found that the debonding load increases with an increasing FRP elastic modulus according to both energy release and ACI methods. When the elastic modulus is too low, the concrete crushing will govern the failure mode of the strengthened beam.

From the above results, the IC debonding load (P_{pred}) increases with increasing concrete compressive strength, FRP reinforcement ratio (except when the amount is too high), tensile steel reinforcement ratio, and elastic modulus of FRP. The possibility of other failure modes, e.g., concrete crusing is also recognized.

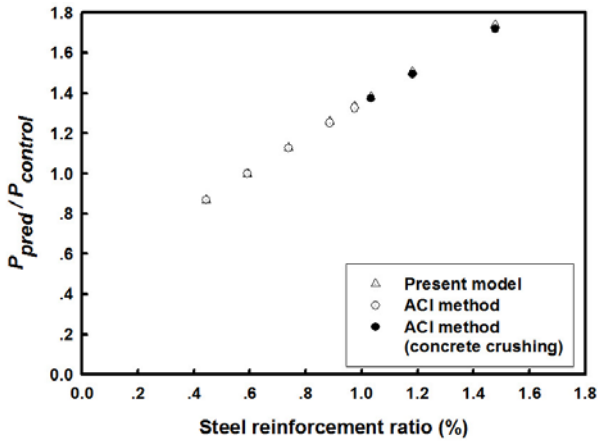

Fig. 10 Effect of steel reinforcement ratio on $P_{pred}/P_{control}$

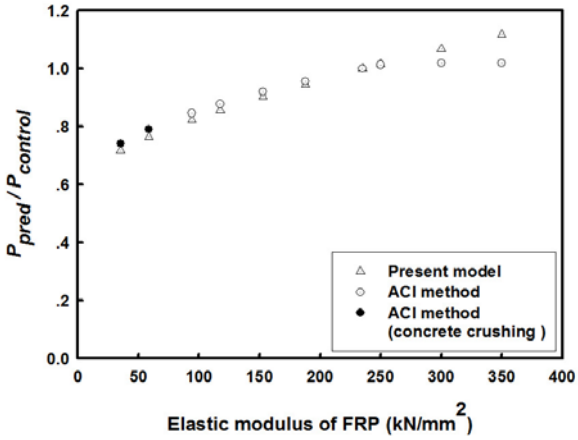

Fig. 11 Effect of FRP modulus on $P_{pred}/P_{control}$

7. Conclusions

This paper presents the analysis of intermediate crack-induced (IC) debonding failure in RC beams strengthened with FRP plates or sheets using the energy release method. The application of ACI model is also presented. The step-by-step procedures for both methods are described in the Appendix A. The effects of relevant parameters on the debonding failure loads are numerically investigated. The main conclusions are as follows,

• Both the energy release and simple ACI methods predict the IC debonding failure loads which are in good agreements with previous experimental data. However, the ACI method predicts a different failure mode, i.e., concrete crushing failure, in some cases.

• Using both analysis methods, the predicted debonding loads increase with the concrete compressive strength, FRP reinforcement ratio, steel reinforcement ratio, and elastic modulus of FRP. However, an increase of FRP reinforcement beyond a specific amount may decrease the debonding load. It is also possible that the failure mode will change from the IC debonding to other failure modes, e.g. concrete crushing.

• Among the studied parameters, the most influential parameter on debonding is the steel reinforcement ratio, followed by FRP reinforcement ratio, elastic modulus of FRP, and concrete compressive strength, respectively.

References

Achinta, P.M.M. and Burgoyne, C.J. (2008), "Fracture mechanics of plate debonding", *J. Compos. Constr.*, **12**(4), 396-404.

Achinta, P.M.M. (2009), "Fracture analysis of debonding mechanism for FRP plates", Ph.D. Dissertation, University of Cambridge, Cambridge.

ACI Committee 440 (2008), *Guide for Design and Construction of Externally Bonded FRP Systems for Strengthening Concrete Structures (ACI 440.2R-08)*, American Concrete Institute, Michigan.

Beber, A.J., Campos Filho, A. and Campagnolo, J.L. (1999), "Flexural strengthening of R/C beams with CFRP sheets", *Proceedings of 8th International Structural Faults and Repair Conference*, London.

Chan, T.K., Cheong, H.K. and Nguyen, D.M. (2001), "Experimental investigation on delamination failure of

CFRP strengthened beams", *Proceedings of ICCMC/IBST 2001 International Conference on Advanced Technologies in Design, Construction and Maintenance of Concrete Structures*, Hanoi, March.
Choi, E., Utui, N. and Kim, H.S. (2013), "Experimental and analytical investigations on debonding of hybrid FRPs for flexural strengthening of RC beams", *Compos. Part B-Eng.*, **45**, 248-256.
Dai, J.G., Harries, K.A. and Yokota, H. (2008), "A critical steel yielding length model for predicting intermediate crack-induced debonding in FRP-strengthened RC members", *Steel Compos. Struct.*, **8**(6), 457-473.
Dai. J.G., Ueda, T. and Sato, Y. (2005), "Development of the nonlinear bond stress–slip model of fiber reinforced plastics sheet-concrete interfaces with a simple method", *J. Compos. Constr.*, **9**(1), 52-62.
Fanning, P.J. and Kelly, O. (2001), "Ultimate response of RC beams strengthened with CFRP plates", *J. Compos. Constr*., **5**(2), 122-127.
Gao, B., Kim, J.K. and Leung, C.Y.K. (2004), "Experimental study on RC beams with FRP strips bonded with rubber modified resins", *Compos. Sci. Technol.*, **64**, 2557-2564.
Guan, G.X., Burgoyne, C.J. and Achintha, M. (2014), "Parametric study of FRP plate debonding using global energy balance", *J. Compos. Constr.*, **18**(6), 04014020.
Gunes, O. (2004), "A fracture based approach to understanding debonding in FRP bonded structural members", Ph.D. Dissertation, Massachusetts Institute of Technology, Massachusetts.
Gunes, O., Buyukozturk, O. and Karaca E. (2009), "A fracture-based model for FRP debonding in strengthened beams", *Eng. Fract. Mech.*, **76**, 1897-1909.
Hao, S.W., Liu, Y. and Liu X.D. (2012), "Improved interfacial stress analysis of a plated beam", *Struct.Eng. Mech*, **44**(6), 815-837.
Kishi, N., Mikami, H., Sato, M. and Matsoka, K. (1998), "Flexural bond behavior of RC beams externally bonded with FRP sheets", *Proceedings of the Japan Concrete Institute*, **20**(1), 515-520.
Lenwari, A., Thepchatri, T. and Albrecht, P. (2005), "Flexural response of steel beams strengthened with partial-length CFRP plates", *J. Compos. Constr.*, **9**(4), 296-303.
Lenwari, A. and Thepchatri, T. (2009), "Experimental study on RC beams strengthened with carbon and glass fiber sheets", *Eng. J.*, **13**(2), 9-18.
Leung, C.K.Y. (2001), "Delamination failure in concrete beams retrofitted with a bonded plate", *J. Mater. Civil Eng.*, **13**, 106-113.
Liu, I.S.T., Oehlers, D.J. and Seracino, R. (2007), "Study of intermediate crack debonding in adhesively plated beams", *J. Compos. Constr.*, **11**(2), 175-183.
Lu, X.Z., Teng, J.G., Ye, L.P. and Jiang, J.J. (2007), "Intermediate crack debonding in FRP-strengthened RC beams: FE analysis and strength model", *J. Compos. Constr.*, **11**(2), 161-174.
Maalej, M. and Leong, K.S. (2005), "Effect of beam size and FRP thickness on interfacial shear stress concentration and failure mode of FRP-strengthened beams", *Compos. Sci. Technol.*, **65**, 1148-1158.
Malek, A.M., Saadatmanesh, H. and Ehsani, M.R. (1998), "Prediction of failure load of R/C beams strengthened with FRP plate due to stress concentration at the plate end", *ACI Struct. J.*, **95**(1), 142-152.
Nakaba, K., Kanakubo, T., Furuta, T. and Yoshizawa, H. (2001), "Bond behavior between fiber-reinforced polymer laminates and concrete", *ACI Struct. J.*, **98**(3), 359-367.
Ombres, L. (2010), "Prediction of intermediate crack debonding failure in FRP-strengthened reinforced concrete beams", *Compos. Struct.*, **92**, 322-329.
Park, R. and Paulay, T. (1975), *Reinforced Concrete Structures*, John Wiley & Sons, New York.
Rahimi, H. and Hutchinson, A. (2001), "Concrete beams with externally bonded FRP plates", *J. Compos. Constr.,* **5**(1), 44-56.
Saadatmanesh, H. and Ehsani, M.R. (1991), "RC beams strengthened with GFRP plates I: experimental study", *J. Struct. Eng.*, **117**(11), 3417-3433.
Said, H. and Wu, Z. (2008), "Evaluating and proposing models of predicting IC debonding failure", *J. Compos. Constr.*, **12**(3), 284-299.
Smith, S.T. and Teng, J.G. (2001), "Interfacial stresses in plated beams", *Eng. Struct.*, **23**, 857-871.
Spadea, G., Bencardino, F. and Swamy, R.N. (1998), "Structural behaviour of composite RC beams with externally bonded CFRP", *J. Compos. Constr.*, **2**(3), 132-137.

Täljsten, B. (1996), "Strengthening of concrete prisms using the plate-bonding technique", *Int. J. Fract.*, **82**, 253-266.
Täljsten, B. (1997), ''Strengthening of beams by plate bonding'', *J. Mater. Civil Eng.*, **9**(4), 206-212.
Teng, J.G., Chen, J.F., Smith, S.T. and Lam, L. (2002), *FRP-Strengthened RC Structures*, John Wiley & Sons, New York.
Teng, J.G., Smith, S.T., Yao, J. and Chen, J.F. (2003), "Intermediate crack-induced debonding in RC beams and slabs", *Constr. Build. Mater.*, **17**, 447-462.
Tumialan, G., Serra, P., Nanni, A. and Belarbi, A. (1999), "Concrete cover delamination in reinforced concrete beams strengthened with carbon fiber reinforced polymer sheets", *Proceedings of the Fourth International Symposium on Fiber Reinforced Polymer Reinforcement for Reinforced Concrete Structures (FRPRCS-4)*, Baltimore, November.
Wang, W.W., Dai, J.G. and Harries, K.A. (2013), "Intermediate crack-induced debonding in RC beams strengthened with prestressed FRP laminates", *J. Reinf. Plast. Comp.*, **32**(23), 1842-1857.
Wantanasiri, P. and Lenwari, A. (2011), "Debonding analysis for RC beams strengthened with FRP plates by energy release concepts", *Proceedings of the 16th National Convention on Civil Engineering*, Chonburi, Thailand, May. (in Thai)
Wu, Z., Yuan, H., and Niu, H. (2002), "Stress transfer and fracture propagation in different kinds of adhesive joints", *J. Eng. Mech.*, **128**(5), 562-573.
Wu, Z. and Niu, H. (2007), "Prediction of crack-induced debonding failure in R/C structures flexurally strengthened with externally bonded FRP composites", *JSCE J. Mater. Concrete Struct. Pave.*, **63**(4), 620-639.
Yuan, H., Teng, J.G., Seracino, R., Wu, Z.S. and Yao, J. (2004), "Full-range behavior of FRP-to-concrete bonded joints", *Eng. Struct.*, **26**, 553-565.
Zhang, L. and Teng, J.G. (2010), "Simple general solution for interfacial stresses in plated beams", *J. Compos. Constr.*, **14**(4), 434-442.

CC

Appendix A. Step-by-step procedures of debonding analysis

A.1 Energy release method

For the energy release method, a step-by-step analysis procedure is given below.

1. Calculate the interfacial fracture energy (G_f)

$$G_f = 0.644 f_c'^{0.19} \tag{A.1}$$

2. Calculate the maximum transferable

$$P_{\max} = b_p \sqrt{2 G_f E_p t_p} \tag{A.2}$$

3. Calculate the effective bond length (L_e)

$$L_e = \frac{0.649 \sqrt{E_p t_p}}{f_c'^{0.095}} \tag{A.3}$$

4. Calculate the equivalent transfer length (L_e')

$$L_e' = 2L_e = \frac{1.3 \sqrt{E_p t_p}}{f_c'^{0.095}} \tag{A.4}$$

5. At the load value P, calculate the FRP tensile forces (f_1) and (f_2) by the section analysis.

6. Check the IC debonding failure criterion as follows, $f_1 - f_1 \geq P_{\max}$.

7. If the above criterion is not satisfied, increase the load value in step 5 until the debonding criterion in step 6 is satisfied. The value of debonding failure load is $P_{deb}=P$.

The possibility of FRP rupture or concrete crushing failure modes which may precede the debonding failure should also be checked.

A.2 ACI method

Fig. A1 shows the section analysis used to construct a simple moment-curvature model. The

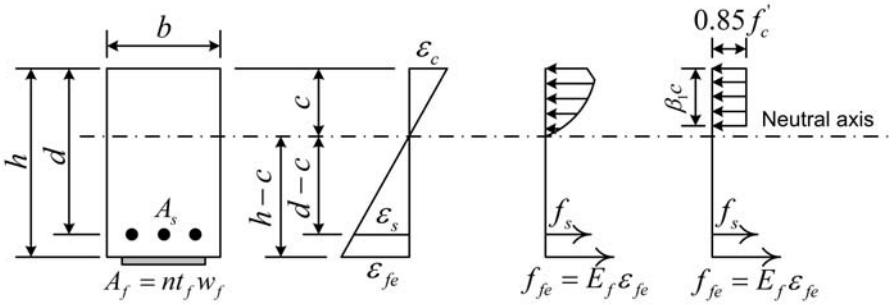

(a) Cross section (b) Strain distribution (c) Stress distribution (d) Equivalent stress block

Fig. A1 Analysis of FRP-strengthened section by ACI method

initial substrate (concrete) strain is assumed to be zero (ε_{bi}=0). A step-by-step analysis procedure for the debonding analysis based on the ACI method is given below.

1. Determine the design ultimate tensile strength (f_{fu}) and design rupture strain (ε_{fu}) of FRP

$$f_{fu} = C_E f^*_{fu} \tag{A.5}$$

$$\varepsilon_{fu} = C_E \varepsilon^*_{fu} \tag{A.6}$$

where f^*_{fu} , ε^*_{fu} and C_E are the ultimate tensile strength of FRP, ultimate rupture strain of FRP, and environmental reduction factor, respectively.

2. Determine the geometric and material properties. The ratio of depth of equivalent rectangular stress block to depth of the neutral axis (β_1) is

$$\beta_1 = \begin{cases} 0.85 & f_c' \le 28 \text{ MPa} \\ 1.05 - 0.007 f_c' & \text{when } 28 < f_c' \le 56 \text{ MPa} \\ 0.65 & f_c' > 56 \text{ MPa} \end{cases} \tag{A.7}$$

where f_c' is the compressive strength of concrete (MPa). The elastic modulus of concrete (E_c) is

$$E_c = 4733\sqrt{f_c'} \qquad \text{(MPa)} \tag{A.8}$$

The tensile steel reinforcement ratio (ρ_s) is

$$\rho_s = \frac{A_s}{bd} \tag{A.9}$$

where A_s, b and d are the area of tensile steel reinforcements, width of beam, and distance from extreme compressive fiber to the centroid of tensile steel reinforcements, respectively. The area of FRP reinforcements (A_f) is

$$A_f = nt_f w_f \tag{A.10}$$

where n, t_f and w_f are the number of layers, nominal thickness of one layer, and width of one layer of FRP reinforcements, respectively. The FRP reinforcement ratio (ρ_f) is

$$\rho_f = \frac{A_f}{bd} \tag{A.11}$$

3. Calculate the debonding strain (ε_{fd}) of FRP reinforcements

$$\varepsilon_{fd} = 0.41\sqrt{\frac{f_c'}{nE_f t_f}} \le 0.9\varepsilon_{fu} \tag{A.12}$$

where E_f is the elastic modulus of FRP.

4. Assume the depth of neutral axis measured from the extreme compression fiber (c).

5. Calculate the effective strain level in FRP reinforcements at failure (ε_{fe})

$$\varepsilon_{fe} = \varepsilon_{cu}\left(\frac{h-c}{c}\right) \tag{A.13}$$

where h and ε_{cu} are the depth of beam and ultimate compressive strain of concrete (=0.003), respectively.

6. Calculate the strain level in tensile steel reinforcements at failure (ε_s)

$$\varepsilon_s = \varepsilon_{fe}\left(\frac{d-c}{h-c}\right) \tag{A.14}$$

7. Determine the corresponding stresses in steel and FRP reinforcements

$$f_s = E_s\varepsilon_s \le f_y \tag{A.15}$$

$$f_{fe} = E_f\varepsilon_{fe} \tag{A.16}$$

where f_y and E_s are the yield strength and elastic modulus of steel reinforcements, respectively.

8. Using an equilibrium condition, the depth of neutral axis from the extreme compression fiber is calculated to be

$$c = \frac{A_s f_s + A_f f_{fe}}{0.85 f_c^{'}\beta_1 b} \tag{A.17}$$

9. If the obtained depth of neutral axis is different from the assumed value, repeat from steps 4 to 8 until the equilibrium condition is satisfied.

10. Check the debonding failure by comparing the effective strain level in FRP reinforcements with the debonding strain limit.

$$\varepsilon_{fe} \le \varepsilon_{fd} \tag{A.18}$$

If the above condition is true, debonding will not govern the failure. Otherwise, the debonding will govern the failure. Back to the step 5 and use the debonding strain limit as the effective strain level in FRP reinforcements.

11. Calculate the nominal flexural strength (M_n) of FRP-strengthened RC beams from

$$M_n = A_s f_s\left(d - \frac{\beta_1 c}{2}\right) + \psi_f A_f f_{fe}\left(h - \frac{\beta_1 c}{2}\right) \tag{A.19}$$

where ψ_f is the FRP strength reduction factor (=0.85).